ADVANCED MATERIALS
www.advmat.de

Microfabricated Ion-Selective Transistors with Fast and Super-Nernstian Response

*Sanggil Han, Shunsuke Yamamoto, Anastasios G. Polyravas, and George G. Malliaras**

Transistor-based ion sensors have evolved significantly, but the best-performing ones rely on a liquid electrolyte as an internal ion reservoir between the ion-selective membrane and the channel. This liquid reservoir makes sensor miniaturization difficult and leads to devices that are bulky and have limited mechanical flexibility, which is holding back the development of high-performance wearable/implantable ion sensors. This work demonstrates microfabricated ion-selective organic electrochemical transistors (OECTs) with a transconductance of 4 mS, in which a thin polyelectrolyte film with mobile sodium ions replaces the liquid reservoir. These devices are capable of selective detection of various ions with a fast response time (≈1 s), a super-Nernstian sensitivity (85 mV dec^{-1}), and a high current sensitivity (224 µA dec^{-1}), comparing favorably to other ion sensors based on traditional and emerging materials. Furthermore, the ion-selective OECTs are stable with highly reproducible sensitivity even after 5 months. These characteristics pave the way for new applications in implantable and wearable electronics.

There is a significant need for miniaturized ion sensors for the real-time monitoring of ion concentrations in applications including fundamental research, health and performance monitoring, agriculture, and safeguarding the food supply and the environment.[1–5] In neuroscience, for example, fast implantable ion sensors could help understand the role of local changes in the extracellular environment in the emergence of seizures.[6] In molecular biology, ion-sensor arrays could potentially enable genome sequencing,[7] identification of single nucleotide polymorphism variants,[8] and real-time monitoring of nucleic acid amplification[9] by measuring hydrogen ions released during nucleotide incorporation. In agriculture, miniaturized sensors inserted in plants, where analytes from soil are purified, could monitor soil nutrients to achieve simultaneous improvements in fertilizer use efficiency and crop yield.[5,10,11] This need has driven the development of new sensor platforms, which has largely focused on transistor-based sensors because of inherent advantages that include facile miniaturization and signal amplification. One of the most studied transistor architectures for ion detection is the ion-sensitive field-effect transistor (ISFET), in which the analyte solution is brought in direct contact with the gate insulator.[1,12,13] A variety of established and emerging materials including silicon, metal oxides, and organics have been investigated in ISFETs, with organics receiving particular attention due to their simple processing, compatibility with flexible substrates, and biocompatibility.[14–16] There has also been recent interest in electrolyte-gated field-effect transistors (EGFETs) that achieve low-voltage sensor operation in aqueous environments.[17–20] In this configuration, a nanometer-thick electrical double layer (EDL) is formed at the electrolyte/channel interface and this provides a high capacitance (typically 1–10 µF cm^{-2}), allowing low-voltage operation. In the case of electrolyte-gated organic field-effect transistors in aqueous environments, the devices normally operate in the water-stable operation window <1 V.[18,19,21] Organic electrochemical transistors (OECTs), in which an ion-transporting organic semiconductor is used as the channel, allow further enhancements in performance.[22] This is due to the fact that changes in doping take place not only near the interface with the analyte, but throughout the bulk of the semiconductor layer. As a result, OECTs show a large transconductance, g_m, that translates to high changes in the drain current (I_D) for small changes in the gate voltage (V_G). This makes OECTs excellent transducers for ionic signals.[23–26]

Selectivity in ion sensors is achieved by employing an ion-selective membrane (ISM) that contains ionophores in a plasticized poly(vinyl chloride) (PVC) matrix.[27] The ionophores interact selectively and reversibly with target ions to form complexes,[28] which provides the ion selectivity. Bulky lipophilic ions (so called "ionic sites") are also embedded in the membrane to facilitate exchange of the target ions while blocking ions of opposite charge through the Donnan exclusion effect.[27] In typical

Dr. S. Han, Prof. S. Yamamoto, A. G. Polyravas, Prof. G. G. Malliaras
Electrical Engineering Division
Department of Engineering
University of Cambridge
9 JJ Thomson Ave, Cambridge CB3 0FA, UK
E-mail: gm603@cam.ac.uk
Prof. S. Yamamoto
Institute of Multidisciplinary Research for Advanced Materials (IMRAM)
Tohoku University
2-1-1 Katahira, Sendai 9808577, Japan
Prof. S. Yamamoto
Department of Biomolecular Engineering
Graduate School of Engineering
Tohoku University
6-6 Aramaki, Aoba, Sendai 9808579, Japan
The ORCID identification number(s) for the author(s) of this article can be found under https://doi.org/10.1002/adma.202004790.

DOI: 10.1002/adma.202004790

ISMs, however, ions have a mobility which is around 1000 times lower than that in aqueous solutions since the presence of the PVC matrix hinders their transport.[29,30] This makes the direct coupling of ISMs with OECTs challenging, as the limited supply of ions to gate the channel leads to poor performance. The ionic conductivity in the membrane can, in principle, be improved by increasing the concentration of ionic sites.[31,32] This was recently leveraged to make OECTs showing a relatively small degradation of the gating performance when coupled directly with ISMs.[4] However, exceeding a molar ratio of ionic site to ionophore beyond an optimal value, typically in the range of 0.2–0.8, is known to deplete free vacant ionophores in the membrane. This degrades the interfacial kinetics for forming ion-ionophore complexes and thus deteriorates the selectivity and sensitivity of the ISM.[28,29,31,33] For this reason, an internal electrolyte reservoir is usually incorporated between the ISM and the channel to supply enough ions to gate the channel effectively and achieve high sensor performance (e.g., sensitivity of 50 μA dec^{-1}).[34,35] However, these liquid or hydrogel electrolyte reservoirs require containment by polydimethylsiloxane (PDMS) or glass chambers, hindering the miniaturization and mechanical flexibility of these devices, therefore, prohibiting their use in wearable/implantable applications. Here, we demonstrate that a thin polyelectrolyte film with mobile sodium ions as the internal ion reservoir enables sensor miniaturization, leading to sensors with fast response time and high sensitivity due to a super-Nernstian response. We show this to be a platform technology, capable of selective detection of different ions by simply using the appropriate ISM. These polyelectrolyte-gated OECTs pave the way for high-performance wearable/implantable ion sensors.

Polyelectrolyte films are polymers consisting of charged polymer chains and mobile counter ions, which leads to ion transport of the counter ions under an applied electric field. We hypothesized that incorporating a polyanionic film with mobile cations between the ISM and the OECT channel would allow a supply of the cations into the channel under a positive gate bias, facilitating efficient gating and addressing the issue of poor ion supply through the ISM. As shown in **Figure 1**a, the proposed ion-selective OECT consists of a channel made of the poly(3,4-ethylenedioxythiophene):poly(styrenesulfonate) (PEDOT:PSS), an internal ion reservoir made of the polyelectrolyte poly(sodium 4-styrenesulfonate) (PSSNa), and an ISM. Details on the device fabrication are provided in the Experimental Section. Figure 1b shows the transfer characteristics of a conventional OECT before and after depositing the ISM and the ion reservoir. The ISM is shown to effectively act as an ion barrier, hindering ions from the analyte solution from permeating into the PEDOT:PSS channel. Indeed, the device in which there is direct contact between the ISM and the channel shows severe degradation of transfer characteristics (red curve). When the PSSNa layer is inserted between the ISM and the channel, the transfer characteristics (blue curve) are similar to those of the original PEDOT:PSS OECT, indicating successful volumetric gating through the mobile Na^+ ions from the PSSNa layer. The channel in the ion-selective OECT is completely dedoped at gate biases >0.85 V and this results in an on/off current ratio of ≈10^5 with an off-state current of ≈20 nA (Figure S1a, Supporting Information), which is a typical behavior of depletion-mode OECTs based on conducting PEDOT:PSS channels.[23] The transfer curves also show small hysteresis (Figure S1b, Supporting Information), which is commonly observed in electrolyte-gated organic transistors.[34,36]

A sodium-selective OECT with 100 nm-channel thickness was fabricated by using an ISM doped with sodium ionophores, exhibiting a maximum g_m of 1.2 mS (see **Figure 2**a). The I_D was recorded at a constant gate and drain voltages (V_G = 0 V, V_D = −0.5 V), while the Na^+ concentration in the analyte was varied in a stepwise manner. An increase in the Na^+ concentration leads to an increase in a potential difference at the interface between the analyte solution and the membrane,[27] and thus more Na^+ ions from the PSSNa layer permeate into and electrochemically dedope the PEDOT:PSS channel, resulting in a decrease in I_D as shown in Figure 2b. To extract sensor parameters, I_D values at equilibrium from Figure 2b and Figure S2a, Supporting Information, were plotted against the Na^+ and K^+ ion concentrations, respectively, as seen in the semilog plot (the left in Figure 2c). Note that the membrane has never been in contact

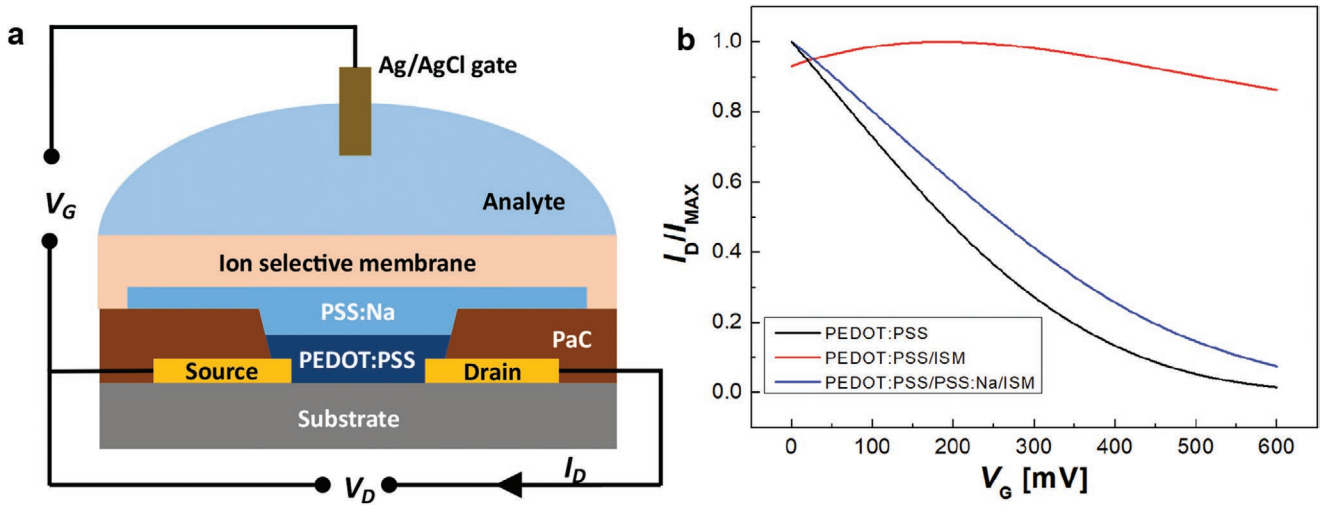

Figure 1. Device structure and electrical characteristics. a) Schematic structure of the ion-selective OECT. b) Transfer characteristics of a conventional OECT before and after coating an ISM, and the final ion-selective OECT.

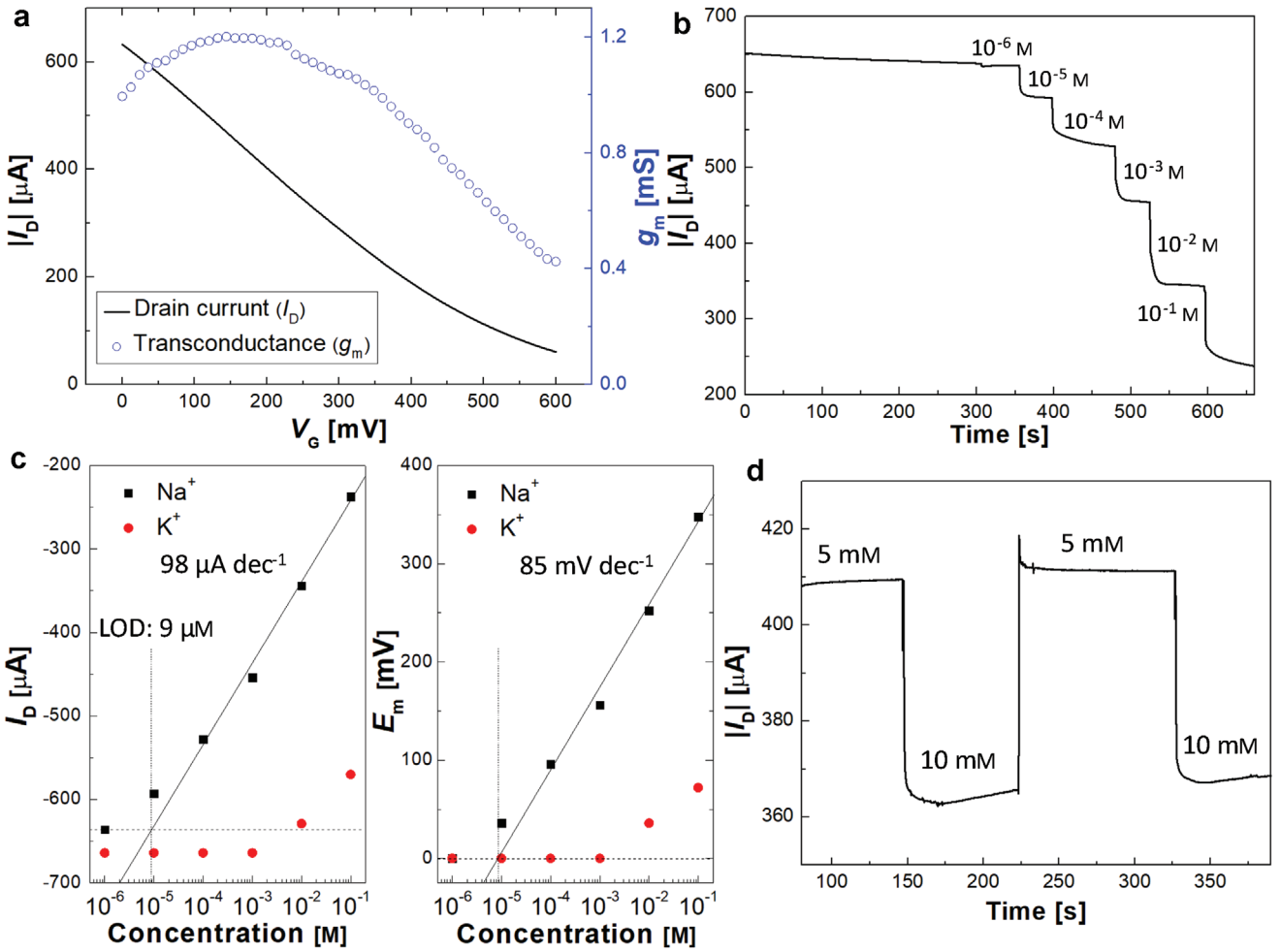

Figure 2. Sodium-selective OECT characteristics and sensor parameters. a) Transfer and transconductance curves measured with DI water at $V_D = -0.5$ V. b) Real-time current response to Na^+ ion concentrations at the fixed $V_G = 0$ V and $V_D = -0.5$ V. c) Calibration curves of the measured current at equilibrium (left) and the calculated membrane potential (right) to NaCl and KCl solutions with different concentrations. d) Dynamic response when Na^+ concentration is changed, going up ($5 \rightarrow 10 \times 10^{-3}$ M) and going down ($10 \rightarrow 5 \times 10^{-3}$ M).

with the primary (Na^+) ions before measuring in a solution of interfering (K^+) ions for obtaining an unbiased selectivity coefficient by minimizing primary ion contamination, and the membrane was also preconditioned in the corresponding ion solutions prior to every measurement.[37] Figure 2c (left) shows that while a relatively small I_D response to K^+ ions is observed from 10^{-2} M, the sodium-selective OECT exhibits a linear response to Na^+ ions in the range of 10^{-4} to 10^{-1} M with a high sensitivity of 98 μA dec^{-1} and a limit of detection (LOD) of $\approx 9 \times 10^{-6}$ M. Here, the LOD was extracted from the intersection point between the linear slope of the calibration curve and the horizontal tangent (dotted line) according to the International Union of Pure and Applied Chemistry definition.[38] Assuming that the membrane activity remains constant, the phase boundary potential at the analyte/membrane interface, simply called the membrane potential, is proportional to the analyte activity (i.e., concentration), which is described by the Nernstian equation as follows,[39]

$$E_m = E^0 + \frac{kT}{ne} \ln\left[M^{n+}\right] \quad (1)$$

where E^0 and $[M^{n+}]$ denote the formal potential and the concentration of the analyte ion, respectively, k is Boltzmann's constant, T is the temperature, n is the valency of the analyte ion, and e is the elementary charge. The E_m values for different ion concentrations were calculated from the transfer curve measured with a blank solution (deionised [DI] water) at the same V_D as shown in Figure 2c (right), showing a super-Nernstian slope of 85 mV dec^{-1}. To obtain the selectivity coefficient, the matched potential method was used, which is based on the activity (concentration) ratio of the primary ion and the interfering ion which leads to the same potential change.[40] The selectivity coefficient was calculated to be $-\log k^{Pot}_{Na,K} = 3.2$ which is a higher value compared to $-\log k^{Pot}_{Na,K} = 1.9$ and $-\log k^{Pot}_{Na,K} = 2.7$ of the sodium-selective electrodes employing the same membrane composition.[41,42] In order to test the sensor reversibility, the Na^+ concentration was increased ($5 \rightarrow 10 \times 10^{-3}$ M) and then decreased ($10 \rightarrow 5 \times 10^{-3}$ M) repetitively in real time as seen in Figure 2d. This shows almost identical I_D when returning back to the previous concentrations, indicating good reversibility.

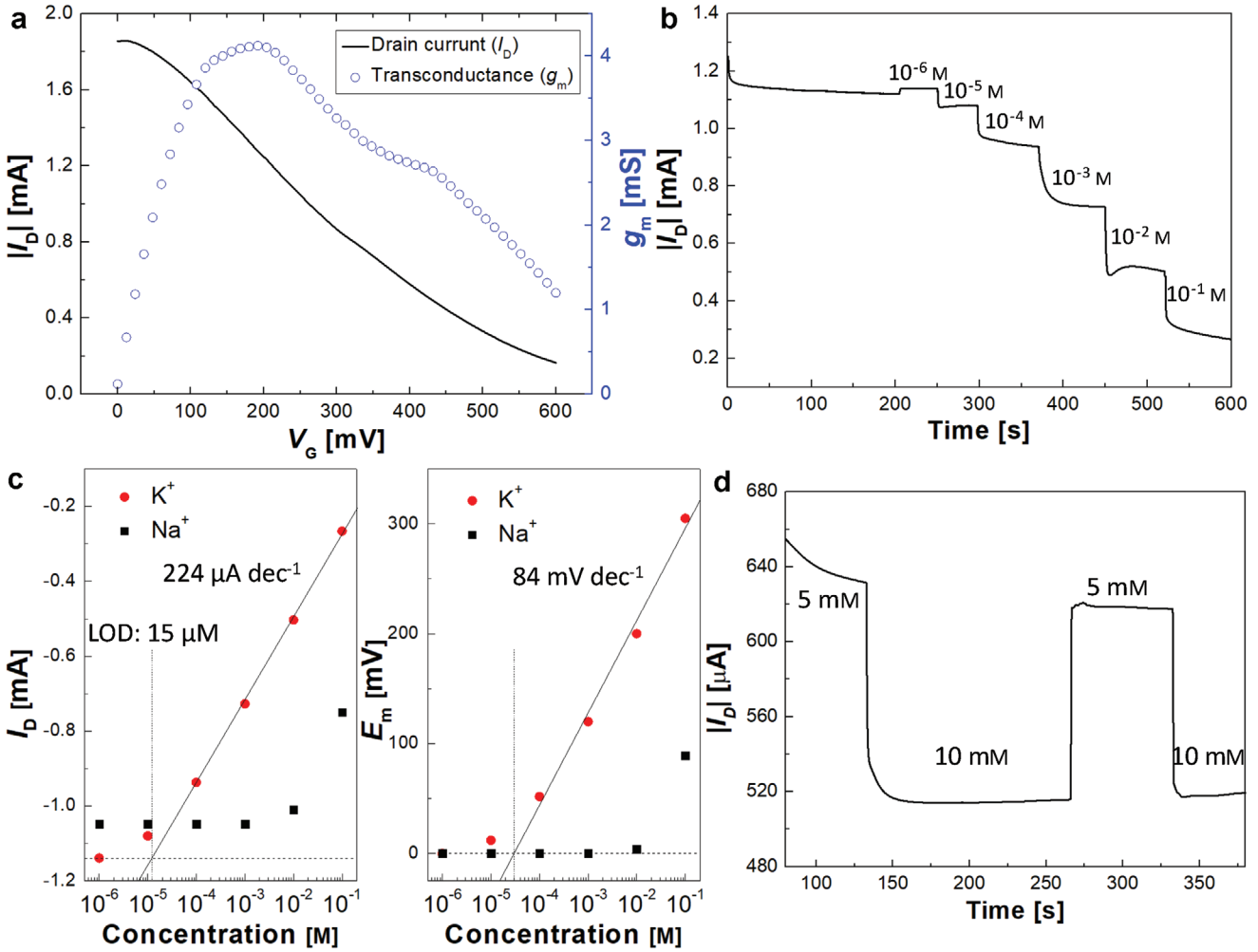

Figure 3. Potassium-selective OECT characteristics and sensor parameters. a) Transfer and transconductance curves measured with DI water at $V_D = -0.4$ V. b) Real-time current response to K^+ ion concentrations at the fixed $V_G = 0.2$ V and $V_D = -0.4$ V. c) Calibration curves of the measured current at equilibrium (left) and the calculated membrane potential (right) to KCl and NaCl solutions with different concentrations. d) Dynamic response when K^+ concentration is changed, going up ($5 \rightarrow 10 \times 10^{-3}$ M) and going down ($10 \rightarrow 5 \times 10^{-3}$ M).

In order to check whether this proposed architecture is generally applicable to the sensing of different ions, a potassium-selective membrane was used instead of the sodium-selective one as seen in Figure 1a. Note that the PEDOT:PSS channel was thicker (250 nm) in this case with the sensor having a maximum g_m of 4 mS (**Figure 3**a).[25] Figure 3b represents the real-time I_D response to various K^+ concentrations. In order to provide a quantitative analysis on the sensor performance, as shown in Figure 3c, calibration curves of the equilibrium I_D measured against the K^+ (Figure 3b) and Na^+ (Figure S2b, Supporting Information) ion concentrations were obtained, and the corresponding E_m values were plotted based on the transfer curve (Figure 3a). Following the same analyses as in the case of the Na^+ sensor, the extracted sensor parameters we found are a super-Nernstian slope of 84 mV dec^{-1}, a sensitivity of 224 μA dec^{-1}, an LOD of 15×10^{-6} M, and a selectivity coefficient of $-\log k^{Pot}_{K,Na} = 2.5$, and the sensor also exhibits a reversible response (see Figure 3d).

The most striking result is that the extracted slope in the linear regime is ≈85 mV dec^{-1} which is higher than the theoretically predicted value of 59.2 mV dec^{-1}. This super-Nernstian response can be understood by considering the mechanism of the operation of the device: The membrane potential at the analyte/ISM interface induces a potential at the ISM/PSSNa interface, which gates the OECT channel through the PSSNa electrolyte. As a result, an increase in the ion concentration of the analyte solution leads to transport of Na^+ ions in the PSSNa layer away from the interface with the ISM and into the PEDOT:PSS channel. The EDL originating from uncompensated PSS^- polyanions at the ISM/PSSNa interface can thus be regarded as an electrochemical gate with a capacitance, C_{DL}, which is connected in series with the capacitance of the channel (C_C). This configuration has been shown to modify the effective gate voltage, resulting in an effective membrane potential[43]

$$E_m^{eff} = E^0 + (1+\gamma)\frac{kT}{ne}\ln\left[M^{n+}\right] \quad (2)$$

where γ is the capacitance ratio defined as $\gamma = C_C/C_{DL}$. The same phenomenon was demonstrated in OECTs operated by a

polarizable gate electrode, showing super-Nernstian response to ion concentration.[26] This means that the super-Nernstian slope depends on device geometry (the capacitance ratio γ), which is supported by the fact that both the Na^+ and K^+ sensors practically show the same sensitivity in mV dec^{-1}. The current sensitivity (i.e., the slope of the linear region on the left in Figures 2c and 3c) can also be predicted from the above equation using the definition of transconductance,

$$g_{m(V_G^{eff})} = \frac{\partial I_D}{\partial E_m^{eff}} = \frac{\partial I_D / \partial \ln[M^+]}{\partial E_m^{eff} / \partial \ln[M^+]} \quad (3)$$

Note that g_m is dependent on the gate voltage as seen in Figure 2a, and thus g_m is a function of the effective gate voltage, $V_G^{eff} = V_G + E_m^{eff}$. For the sodium-selective OECT, since V_G = 0 V and 100 mV < E_m^{eff} < 350 mV in the linear region on the right in Figure 2c, V_G^{eff} varies between 100 and 350 mV, resulting in g_m ≈1–1.2 mS (see Figure 2a). Using Equation (3) and $\partial E_m^{eff}/\partial \ln[M^+]$ = 85 mV dec^{-1}, the current sensitivity ($\partial I_D/\partial \ln[M^+]$) is calculated to be 85–102 µA dec^{-1}. For the potassium-selective OECT, as V_G = 200 mV and 50 mV < E_m^{eff} < 300 mV in the linear region on the right in Figure 3c, V_G^{eff} varies from 250 to 500 mV, giving g_m ≈2–3.5 mS (see Figure 3a)

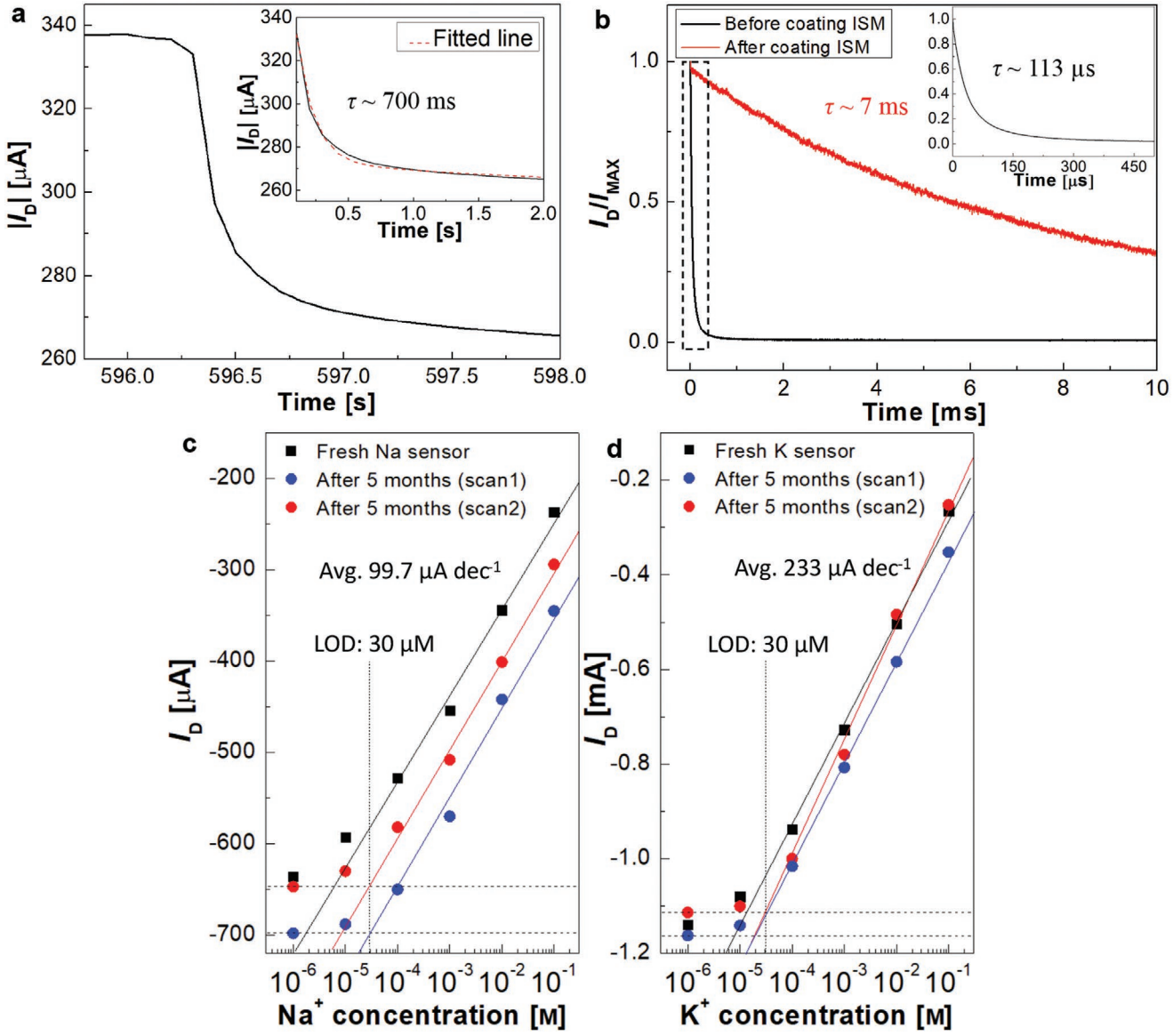

Figure 4. Response time and sensor stability. a) Current response of the sodium-selective OECT to a sudden change in Na^+ concentration from 10^{-2} to 10^{-1} M at the fixed V_G = 0 V and V_D = –0.5 V. Inset shows a fitted line of the curve performed using a double-exponential decay function, resulting in a time constant of ≈700 ms. b) Normalized temporal response of I_D of the PSSNa-coated OECT before (black) and after forming the ISM (red) in response to pulsed V_G of 500 mV. Inset magnifies the region of the I_D response enclosed by the black dashed line. The ion-injection time constants before and after coating the ISM were calculated to be 133 µs and 7 ms, respectively. c,d) Calibration curves for repetitive scans of the Na^+ sensor (c) and the K^+ sensor (d). The sensitivity values (slopes) are 98 µA dec^{-1} (black squares), 97 µA dec^{-1} (blue circles), and 104 µA dec^{-1} (red circles) in (c) and 224 µA dec^{-1} (black squares), 222 µA dec^{-1} (blue circles), and 254 µA dec^{-1} (red circles) in (d).

Table 1. Performance comparison with several ion-selective transistor technologies.

Technologies	Analytes	E_m sensitivity [mV dec^{-1}]	I_D sensitivity [μA dec^{-1}]	$-\log k_{i,J}^{Pot}$	LOD [× 10^{-6} M]	Response time [s]	V_{MAX}[a)] [V]	References
ISE	Na^+	≈59	–	1.9, 2.7	3.5, 10	<20	–	[41,42]
Si ISFET	Ca^{2+}, K^+	26.5, 55.7	–	2	1, 40	–	–	[10]
Graphene ISFET	K^+	63.6	35	–	1	≈7	1	[53]
AlGaN/GaN ISHEMT[b)]	Pb^{2+}	36	7	–	10^{-3}	–	1	[54]
Dual-gated ISFET	Cu^{2+}	98	0.033	–	10^{-8}	–	17	[45]
EGOFET[c)]	Na^+	62	0.5	–	1	≈30	0.2	[34]
OECT w/o internal electrolyte	NH_4^+, Ca^{2+}	–	0.06, 0.03	–	≈10	<10	0.2	[4]
OECT with internal electrolyte	K^+	48	47	2.7	≈10	36	0.7	[35]
OECT with PSSNa electrolyte	Na^+, K^+	≈85	98 224	3.2, 2.5	≈10	≈1	0.5	This work

[a)]Maximum applied voltage; [b)]Ion-selective high electron mobility transistor; [c)]Electrolyte-gated organic field-effect transistor.

and thus the resultant current sensitivity is expected to be 168–294 μA dec^{-1}. The experimentally obtained values for sensitivity of 98 μA dec^{-1} (Na^+ sensor) and 224 μA dec^{-1} (K^+ sensor) are within the predicted range based on Equation (3).

In order to provide a quantitative analysis on the response time, as seen in **Figure 4**a, a time constant (τ) was calculated by fitting the I_D response of the sodium-selective OECT to a change in Na^+ concentration from 10^{-2} to 10^{-1} M with a double-exponential decay function, $I_D = I_0 + A_1 e^{-t/\tau_1} + A_2 e^{-t/\tau_2}$, and using the amplitude-weighted average method (i.e., $\tau = (A_1\tau_1 + A_2\tau_2)/(A_1 + A_2)$), resulting in $\tau \approx 700$ ms. The average time constant (τ_{avg}) of the τ values extracted from every step change in I_D (Figure 2b) was obtained to be $\tau_{avg} \approx 1.3$ s which is a much faster value compared to those ($\tau > 30$ s) of the previously reported ion-selective EGFET[34] and OECT[35] using a bulky liquid or hydrogel as an internal electrolyte reservoir. The response time of the ion-selective OECTs can be limited by the three equilibrium processes: 1) ion diffusion across the stagnant solution, 2) ion complexation with ionophores at the membrane surface, and 3) ion injection from the internal electrolyte into the channel. As shown in Figure 4b, the temporal responses of I_D were recorded with a fixed Na^+ concentration (10^{-1} M) by applying the gate pulse in the direction of the ion injection, which allows extraction of the time constant related to the ion injection into the channel. Upon introduction of the ISM, the time constant increased from 113 μs to ≈7 ms. This suggests that the ion injection from PSSNa into the channel is not the dominant factor limiting the response time, and thus this polyelectrolyte-gated ion-selective OECT has room for improvement by equipping it with a flow cell to reduce ion diffusion time in the analyte solution and/or by optimizing the ISM composition to improve the interfacial kinetics for forming ion-ionophore complexes.

In order to investigate the sensor stability, repetitive measurements of I_D versus concentration were performed after 5 months of storage in ambient dry conditions (Figure S3, Supporting Information), and the corresponding calibration curves were obtained as seen in Figure 4c (Na^+ sensor) and Figure 4d (K^+ sensor). Although a fluctuation of the baseline current, <10% (Na^+) and <4% (K^+), is observed, the devices exhibit stable sensor performance with highly reproducible sensitivity (average values of 99.7 μA dec^{-1} (Na^+) and 233 μA dec^{-1} (K^+)) in the range of the linear response (10^{-4}–10^{-1} M). The LOD increases slightly to 30×10^{-6} M after 5 months, which is also observed in the ISM lifetime tests.[44] The results indicate that the sensors have a remarkably long lifetime and show stable sensitivity.

The performance of the polyelectrolyte-gated OECTs is compared with several ion-selective transistor technologies, along with typical values for ion-selective electrodes (ISEs), in **Table 1**. The super-Nernstian response can also be observed in dual-gated transistors (e.g., 98 mV dec^{-1} for a divalent ion, Cu^{2+})[45] and the sensitivity in this configuration can be adjusted by the ratio of the top and bottom gate capacitances.[16,46,47] However, dynamic (i.e., real-time) responses have never been reported in the existing literature on the dual-gated ISFETs.[45,48–52] The overall performance of the sensors reported here surpasses that of all transistor technologies, in particular, in terms of the current sensitivity and response time. Perhaps the most striking result we obtained here is that the current sensitivity depends on g_m and hence can be easily increased by controlling g_m through, for example, tuning of channel thickness. The fast response is due to a reduction in ionic resistance resulting from a thin internal electrolyte layer, along with a fast OECT. Together with the fact that the sensor architecture is generic and can be easily coupled with other ISMs to sense different ions, the results shown open new frontiers for the applications of ion sensors.

Experimental Section

Materials: PEDOT:PSS (Clevios PH1000) and Micro-90 cleaning solution were purchased from Heraeus and Cole–Parmer, respectively. Ethylene glycol, 4-dodecylbenzenesulfonic acid (DBSA), (3-glycidyloxypropyl)trimethoxysilane (GOPS), PSSNa (molecular weight ≈1 000 000), 3-(trimethoxysilyl)propyl methacrylate (Silane A174), high-molecular-weight PVC, 2-nitrophenyl octyl ether (2-NPOE), potassium tetrakis(4-chlorophenyl)borate (KT_4ClPB), sodium ionophore X, potassium ionophore III, tetrahydrafuran (THF), sodium chloride (NaCl), and potassium chloride (KCl) were acquired from Sigma-Aldrich and were used without further purification.

Polymer Blend Preparation: The PEDOT:PSS blend was prepared by adding 5 vol% ethylene glycol (to improve film conductivity), 0.25 vol% DBSA (to improve film homogeneity), and 1 vol% GOPS (as a crosslinker) to a stock PEDOT:PSS solution. The ISM solution was prepared by mixing high molecular weight PVC (33 wt%), plasticizer (2-NPOE, 66.1 wt%), cation exchanger (KT_4ClPB, 0.2 wt%), and a corresponding ionophore in THF (400 mg/4 mL). Sodium ionophore X (0.7 wt%) and potassium ionophore III (2 wt%) were used to prepare the sodium and potassium-selective membrane, respectively. The resultant molar ratio of the ionic site (KT_4ClPB) to ionophore was 0.22 (for sodium) and 0.77 (for potassium) which were in the range of the optimal value (0.2–0.8). For the PSSNa mixture, 1 M HCl (1 vol%), DBSA (0.25 vol%), and GOPS (1 vol%) were added to a 1.2 w/v% PSSNa solution. HCl was added to modify pH to enhance the crosslinking reaction.[55]

Device Fabrication: OECTs were fabricated as recently reported (see a detailed fabrication process).[56] Briefly, source/drain electrodes and interconnects were formed on cleaned glass substrates by e-beam evaporation (Kurt J. Lesker PVD-75) of a Ti (5 nm)/Au (100 nm) layer and the lift-off process. A 2 µm-thick parylene C was deposited on the samples to electrically isolate the electrodes after a surface treatment using Silane A-174, an adhesion promoter. A diluted Micro-90 (2% v/v in DI water) was spin-coated as an antiadhesive layer, and subsequently, a sacrificial second parylene C layer of 2 µm was deposited. The OECT channels, with the width and length of both 50 µm, and contact pads were opened through successive photolithography and reactive ion etching steps (Oxford 80 Plasmalab plus). After surface activation by oxygen plasma, the PEDOT:PSS blend filtered through a 0.45 µm polytetrafluoroethylene filter was spin-coated on the sample at 3000 rpm. The sacrificial parylene layer was peeled off to pattern the OECT channels, and then the sample was baked at 130 °C for 60 min to make a crosslinked PEDOT:PSS film and immersed in DI water overnight to remove any excess compounds. The PSSNa mixture was spin-coated on the PEDOT:PSS channels at 1000 rpm, and then the polyelectrolyte film with GOPS was crosslinked by baking at 130 °C for 60 min and subsequently immersed in a 100×10^{-3} M NaCl solution overnight to keep Na ions in the film while removing any excess compounds such as DBSA. Finally, the ISM solution was drop-cast on top of the PSSNa film and dried at room temperature to make the ISM film (≈30 µm).

Device Characterization: A small PDMS well was placed on top of the ISM to confine an analyte solution. All the electrical measurements were performed using a semiconductor device analyzer (Keysight B1500A) and an Ag/AgCl pellet (World Precision Instruments) as a gate electrode inside a Faraday cage in ambient conditions (40% relative humidity at 20 °C) and ambient light. For obtaining real-time responses (I_D–time) to the stepwise increase in ion concentrations, the PDMS well was first filled with DI water of 50 µL, and then I_D was recorded at constant V_G and V_D. After the baseline current was stabilized, either the Na^+ or K^+ concentration was increased by successively adding the corresponding NaCl and KCl solutions (10^{-5} to 1 M) to the DI water in the well at a 1:10 ratio of the total volume. For the reversibility tests, a chamber (2 mL volume) with a bottom hole was placed on the PDMS well. The ion concentration in the chamber was adjusted from 5 to 10×10^{-3} M by adding a calculated amount of the 100×10^{-3} M solution, and from 10 to 5×10^{-3} M by diluting it with DI water.

Supporting Information

Supporting Information is available from the Wiley Online Library or from the author.

Acknowledgements

This work was supported by the King Abdullah University of Science and Technology (KAUST) Office of Sponsored Research (OSR) under award no. OSR-2016-CRG5-3003 and by the Natural Environment Research Council (NERC) under award no. NE/T012293/1.

Conflict of Interest

The authors declare no conflict of interest.

Keywords

ion sensors, ion-selective transistors, organic electrochemical transistors, polyelectrolyte gating, super-Nernstian sensitivity

Received: July 14, 2020
Revised: August 26, 2020
Published online: October 29, 2020

[1] A. Bratov, N. Abramova, A. Ipatov, *Anal. Chim. Acta* **2010**, *678*, 149.
[2] O. Knopfmacher, M. L. Hammock, A. L. Appleton, G. Schwartz, J. Mei, T. Lei, J. Pei, Z. Bao, *Nat. Commun.* **2014**, *5*, 2954.
[3] W. Gao, S. Emaminejad, H. Y. Y. Nyein, S. Challa, K. Chen, A. Peck, H. M. Fahad, H. Ota, H. Shiraki, D. Kiriya, D.-H. Lien, G. A. Brooks, R. W. Davis, A. Javey, *Nature* **2016**, *529*, 509.
[4] S. T. Keene, D. Fogarty, R. Cooke, C. D. Casadevall, A. Salleo, O. Parlak, *Adv. Healthcare Mater.* **2019**, *8*, 1901321.
[5] C. Jimenez, J. Orozco, A. Baldi, *Sensors* **2010**, *10*, 61.
[6] J. V. Raimondo, R. J. Burman, A. A. Katz, C. J. Akerman, *Front. Cell. Neurosci.* **2015**, *9*, 419.
[7] J. M. Rothberg, W. Hinz, T. M. Rearick, J. Schultz, W. Mileski, M. Davey, J. H. Leamon, K. Johnson, M. J. Milgrew, M. Edwards, J. Hoon, J. F. Simons, D. Marran, J. W. Myers, J. F. Davidson, A. Branting, J. R. Nobile, B. P. Puc, D. Light, T. A. Clark, M. Huber, J. T. Branciforte, I. B. Stoner, S. E. Cawley, M. Lyons, Y. Fu, N. Homer, M. Sedova, X. Miao, B. Reed, J. Sabina, E. Feierstein, M. Schorn, M. Alanjary, E. Dimalanta, D. Dressman, R. Kasinskas, T. Sokolsky, J. A. Fidanza, E. Namsaraev, K. J. McKernan, A. Williams, G. T. Roth, J. Bustillo, *Nature* **2011**, *475*, 348.
[8] C. Toumazou, L. M. Shepherd, S. C. Reed, G. I. Chen, A. Patel, D. M. Garner, C.-J. A. Wang, C.-P. Ou, K. Amin-Desai, P. Athanasiou, H. Bai, I. M. Q. Brizido, B. Caldwell, D. Coomber-Alford, P. Georgiou, K. S. Jordan, J. C. Joyce, M. L. Mura, D. Morley, S. Sathyavruthan, S. Temelso, R. E. Thomas, L. Zhang, *Nat. Methods* **2013**, *10*, 641.
[9] B. Veigas, J. Pinto, R. Vinhas, T. Calmeiro, R. Martins, E. Fortunato, P. V. Baptista, *Biosens. Bioelectron.* **2017**, *91*, 788.
[10] J. Artigas, A. Beltrán, C. Jiménez, A. Baldi, R. Mas, C. Domínguez, J. Alonso, *Comput. Electron. Agric.* **2001**, *31*, 281.
[11] T. H. Gieling, G. van Straten, H. J. J. Janssen, H. Wouters, *Sens. Actuators B* **2005**, *105*, 74.
[12] P. Bergveld, *IEEE Trans. Biomed. Eng.* **1970**, *BME-17*, 70.
[13] P. Bergveld, *Sens. Actuators B* **2003**, *88*, 1.
[14] M. Yano, K. Koike, K. Mukai, T. Onaka, Y. Hirofuji, K.-I. Ogata, S. Omatu, T. Maemoto, S. Sasa, *Phys. Status Solidi A* **2014**, *211*, 2098.
[15] J. T. Mabeck, G. G. Malliaras, *Anal. Bioanal. Chem.* **2006**, *384*, 343.
[16] M.-J. Spijkman, J. J. Brondijk, T. C. T. Geuns, E. C. P. Smits, T. Cramer, F. Zerbetto, P. Stoliar, F. Biscarini, P. W. M. Blom, D. M. de Leeuw, *Adv. Funct. Mater.* **2010**, *20*, 898.
[17] S. H. Kim, K. Hong, W. Xie, K. H. Lee, S. Zhang, T. P. Lodge, C. D. Frisbie, *Adv. Mater.* **2013**, *25*, 1822.
[18] L. Kergoat, L. Herlogsson, D. Braga, B. Piro, M.-C. Pham, X. Crispin, M. Berggren, G. Horowitz, *Adv. Mater.* **2010**, *22*, 2565.
[19] F. Buth, D. Kumar, M. Stutzmann, J. A. Garrido, *Appl. Phys. Lett.* **2011**, *98*, 153302.
[20] I. Cunha, R. Barras, P. Grey, D. Gaspar, E. Fortunato, R. Martins, L. Pereira, *Adv. Funct. Mater.* **2017**, *27*, 1606755.

[21] M. Braendlein, T. Lonjaret, P. Leleux, J.-M. Badier, G. G. Malliaras, *Adv. Sci.* **2016**, *4*, 1600247.
[22] J. Rivnay, S. Inal, A. Salleo, R. M. Owens, M. Berggren, G. G. Malliaras, *Nat. Rev. Mater.* **2018**, *3*, 17086.
[23] J. Rivnay, P. Leleux, M. Sessolo, D. Khodagholy, T. Hervé, M. Fiocchi, G. G. Malliaras, *Adv. Mater.* **2013**, *25*, 7010.
[24] D. Khodagholy, J. Rivnay, M. Sessolo, M. Gurfinkel, P. Leleux, L. H. Jimison, E. Stavrinidou, T. Herve, S. Sanaur, R. M. Owens, G. G. Malliaras, *Nat. Commun.* **2013**, *4*, 2133.
[25] J. Rivnay, P. Leleux, M. Ferro, M. Sessolo, A. Williamson, D. A. Koutsouras, D. Khodagholy, M. Ramuz, X. Strakosas, R. M. Owens, C. Benar, J.-M. Badier, C. Bernard, G. G. Malliaras, *Sci. Adv.* **2015**, *1*, e1400251.
[26] P. Lin, F. Yan, H. L. W. Chan, *ACS Appl. Mater. Interfaces* **2010**, *2*, 1637.
[27] C. Bieg, K. Fuchsberger, M. Stelzle, *Anal. Bioanal. Chem.* **2017**, *409*, 45.
[28] S. Amemiya, in *Handbook of Electrochemistry* (Ed: C. G. Zoski), Elsevier, Amsterdam, The Netherlands **2007**, pp. 261–294.
[29] R. D. Armstrong, *Electrochim. Acta* **1987**, *32*, 1549.
[30] R. D. Armstrong, G. Horvai, *Electrochim. Acta* **1990**, *35*, 1.
[31] E. Pretsch, D. Wegmann, D. Ammann, A. Bezegh, O. Dinten, M. W. Läubli, W. E. Morf, U. Oesch, K. Sugahara, H. Weiss, W. Simon, in *Ion Measurements in Physiology and Medicine* (Eds: M. Kessler, D. K. Harrison, J. Hoper), Springer, Berlin, Germany **1985**, pp. 11–16.
[32] B. D. Pendley, R. E. Gyurcsanyi, R. P. Buck, E. Lindner, *Anal. Chem.* **2001**, *73*, 4599.
[33] U. Schaller, E. Bakker, U. E. Spichiger, E. Pretsch, *Anal. Chem.* **1994**, *66*, 391.
[34] K. Schmoltner, J. Kofler, A. Klug, E. J. W. List-Kratochvil, *Adv. Mater.* **2013**, *25*, 6895.
[35] M. Sessolo, J. Rivnay, E. Bandiello, G. G. Malliaras, H. J. Bolink, *Adv. Mater.* **2014**, *26*, 4803.
[36] G. Tarabella, P. D'Angelo, A. Cifarelli, A. Dimonte, A. Romeo, T. Berzina, V. Erokhin, S. Iannotta, *Chem. Sci.* **2015**, *6*, 2859.
[37] E. Lindner, Y. Umezawa, *Pure Appl. Chem.* **2008**, *80*, 85.
[38] R. P. Buck, E. Lindner, *Pure Appl. Chem.* **1994**, *66*, 2527.
[39] G. A. Crespo, E. Bakker, *RSC Adv.* **2013**, *3*, 25461.
[40] E. Bakker, E. Pretsch, P. Buhlmann, *Anal. Chem.* **2000**, *72*, 1127.
[41] A. M. Cadogan, D. Diamond, M. R. Smyth, M. Deasy, M. A. McKervey, S. J. Harris, *Analyst* **1989**, *114*, 1551.
[42] A. Cadogan, Z. Gao, A. Lewnstam, A. Ivaska, D. Diamond, *Anal. Chem.* **1992**, *64*, 2496.
[43] D. A. Bernards, D. J. Macaya, M. Nikolou, J. A. DeFranco, S. Takamatsu, G. G. Malliaras, *J. Mater. Chem.* **2008**, *18*, 116.
[44] O. T. Guenat, S. Generelli, N. F. de Rooij, M. Koudelka-Hep, F. Berthiaume, M. L. Yarmush, *Anal. Chem.* **2006**, *78*, 7453.
[45] A. Kenaan, F. Brunel, J. M. Raimundo, A. M. Charrier, *Sens. Actuators B* **2020**, *316*, 128147.
[46] N. Liu, R. Chen, Q. Wan, *Sensors* **2019**, *19*, 3425.
[47] Y.-C. Syu, W.-E. Hsu, C.-T. Lin, *ECS J. Solid State Sci. Technol.* **2018**, *7*, Q3196.
[48] O. Knopfmacher, A. Tarasov, W. Fu, M. Wipf, B. Niesen, M. Calame, C. Schonenberger, *Nano Lett.* **2010**, *10*, 2268.
[49] M. Spijkman, E. C. P. Smits, J. F. M. Cillessen, F. Biscarini, P. W. M. Blom, D. M. de Leeuw, *Appl. Phys. Lett.* **2011**, *98*, 043502.
[50] C. Duarte-Guevara, F.-L. Lai, C.-W. Cheng, B. Reddy, E. Salm, V. Swaminathan, Y.-K. Tsui, H. C. Tuan, A. Kalnitsky, Y.-S. Liu, R. Bashir, *Anal. Chem.* **2014**, *86*, 8359.
[51] N. Liu, Y. H. Liu, P. Feng, L. Q. Zhu, Y. Shi, Q. Wan, *Appl. Phys. Lett.* **2015**, *106*, 073507.
[52] N. Kumar, J. Kumar, S. Panda, *IEEE Electron Device Lett.* **2016**, *37*, 500.
[53] H. Li, Y. Zhu, Md. S. Islam, Md. A. Rahman, K. B. Walsh, G. Koley, *Sens. Actuators B* **2017**, *253*, 759.
[54] Y.-T. Chen, I. Sarangadharan, R. Sukesan, C.-Y. Hseih, G.-Y. Lee, J.-I. Chyi, Y.-L. Wang, *Sci. Rep.* **2018**, *8*, 8300.
[55] A. Håkansson, S. Han, S. Wang, J. Lu, S. Braun, M. Fahlman, M. Berggren, X. Crispin, S. Fabiano, *J. Polym. Sci., Part B: Polym. Phys.* **2017**, *55*, 814.
[56] A. G. Polyravas, V. F. Curto, N. Schaefer, A. B. Calia, A. Guimera-Brunet, J. A. Garrido, G. G. Malliaras, *Flexible Printed Electron.* **2019**, *4*, 044003.